UAV - 3: Patrol

Mariana Alves Pires (102939)
Tiago Cruz Clamote (103285)
Lourenço Gouveia Faria (103354)

Prof. José Raul Carreira Azinheira

Instituto Superior Técnico, Lisboa, Portugal

March 2024

Abstract

This report was made in the context of the course 'Flight Control' from the bachelor's degree in Aerospace Engineering from Instituto Superior Técnico. The results presented throughout the paper were obtained using MATLAB® and the vehicle's characteristics were imported from the project's reference paper. The aircraft under study is a UAV and there will be an emphasis in the analysis of the roll and sideslip angle stability, stability augmentation, attitude and trajectory control, actuator and sensor modeling, and the simulation of a patrol maneuver.
Keywords: UAV, patrol

1. Introduction

This project aimed to delve into the dynamic and kinematic models of a UAV aircraft. The sideslip and roll angles will be given special attention and, therefore, the lateral behaviour of the vehicle will be analysed with great detail. The report will involve an in-depth analysis of the aircraft's stability while applying methods to improve it (SAS), experimentation with a control system, modulation of an actuation system and sensors, and simulation of a patrol mission.

2. Determination and analysis of the studied model

In order to analyze the lateral movement of the aircraft, the following linearized model of the motion equations was considered [1], represented within the framework of the dynamic space:

$$\begin{cases} \dot{v} = Y_v v + (Y_p + W_0)p + (Y_r - U_0)r + g_{c\theta_0}\phi + Y_{\delta R}\delta R \\ \dot{p} - \frac{I_{xz}}{I_{xx}}\dot{r} = L_v v + L_p p + L_r r + L_{\delta A}\delta A + L_{\delta R}\delta R \\ \dot{r} - \frac{I_{xz}}{I_{zz}}\dot{p} = N_v v + N_p p + N_r r + N_{\delta A}\delta A + N_{\delta R}\delta R \\ \dot{\phi} = p + t_{\theta_0} r \end{cases}$$

In this system, it's important to highlight that the equation governing the yaw angle is absent. This is because ψ acts solely as a pure integrator of the other states, exerting no influence on them. Henceforth, as the variation of ψ is not under scrutiny, the system is effectively modeled as a fourth-order system.

The stability derivatives can be simplified in the following way:

$$L_i^{'} = L_i + \frac{I_{xz}}{I_{xx}} N_i$$

$$N_j^{'} = N_j + \frac{I_{xz}}{I_{zz}} L_j$$

This way, assuming that the system is linear time invariant (LTI), the expression for the aircraft dynamic equations for the 4^{th} order model is obtained:

$$\dot{x} = Ax + Bu$$

The dynamic and control matrices A and B can be defined as:

$$\mathrm{A} = \begin{bmatrix} Y_v & Y_p + W_0 & Y_r - U_0 & g\cos\theta_0 \\ L_v^{'} & L_p^{'} & L_r^{'} & 0 \\ N_v^{'} & N_p^{'} & N_r^{'} & 0 \\ 0 & 1 & \tan\theta_0 & 0 \end{bmatrix} \quad \mathrm{B} = \begin{bmatrix} Y_{\delta_A} & Y_{\delta_R} \\ L_{\delta_A}^{'} & L_{\delta_R}^{'} \\ N_{\delta_A}^{'} & N_{\delta_R}^{'} \\ 0 & 0 \end{bmatrix}$$

Here $x = [v \ p \ r \ \phi]^T$ is the state space and $u = [\delta_A \ \delta_R]^T$ the inputs.

Since the ailerons mainly influence the longitudinal movement, the effect of Y_{δ_A} is neglected.

Given the aircraft properties [2], the derivatives provided already consider the state β. Therefore, the space state is better described as $x = [\beta \ p \ r \ \phi]^T$.

For small angles, the velocity is given by the expression $v = \beta U_0$. In order to implement the required adjustments, the first row of matrices A and B needs to be divided by U_0. However, it's important to note that only the non-derivative components in matrix A require modification. This is because the derivatives in matrix B and within matrix A already incorporate this division [2]. This way, the following matrices $A_{(4\times4)}$ and $B_{(4\times2)}$ are obtained:

$$\mathrm{A} = \begin{bmatrix} Y_\beta & Y_p + \tan\alpha_0 & Y_r - 1 & \frac{g\cos\theta_0}{U_0} \\ L'_\beta & L'_p & L'_r & 0 \\ N'_\beta & N'_p & N'_r & 0 \\ 0 & 1 & \tan\theta_0 & 0 \end{bmatrix} \quad \mathrm{B} = \begin{bmatrix} Y_{\delta_A} & Y_{\delta_R} \\ L'_{\delta_A} & L'_{\delta_R} \\ N'_{\delta_A} & N'_{\delta_R} \\ 0 & 0 \end{bmatrix}$$

When substituting each variable with its respective value from the project's reference paper [2], the following matrices are derived:

$$A = \begin{bmatrix} -0.1531 & 0.0070 & -1.0000 & 0.4674 \\ -60.8700 & -17.9173 & 5.9768 & 0 \\ 19.9554 & -1.8931 & -0.2096 & 0 \\ 0 & 1.0000 & 0.0070 & 0 \end{bmatrix}$$

$$B = \begin{bmatrix} 0 & -0.0070 \\ -73.6300 & 1.4329 \\ -1.9235 & 22.1810 \\ 0 & 0 \end{bmatrix}$$

The system's poles are the eigenvalues of the dynamic matrix A, which are obtained from the characteristic equation $\Delta(s) = \mathrm{Det}(sI - A) = 0$. For this, the characteristic polynomial is given by $\Delta(s) = s^2 + 2\xi w_n + w_n^2$. Using the command *damp* for the matrix A, the following results were obtained:

Flight modes	poles	ξ	w_n $[rad/s]$	time const.[s]
Spiral divergence	0.101	-1.00	0.101	-9.87
Dutch roll	$-0.324 \pm 5.34i$	0.0607	5.35	3.08
Roll subsidence	-17.7	1.00	17.7	0.0564

Table 1: Lateral mode results

Flight characteristics

In order to assess the flight characteristics of the aircraft, the assessment grids found in the course bibliography [1] were used. Consequently, the aircraft was identified as belonging to either class I or IV (maneuverable airplane weighing less than 5000 kg) and falling under category A (non-terminal flight phase, involving rapid maneuvers and/or precise trajectory control). For the following conclusions, it will be assumed class IV (even though conclusions would remain the same if assumed class I).

Spiral Divergence

Likewise, the evaluation process was conducted in terms of levels. For the spiral divergence mode, which is characterized by instability, was imperative to determine the time $T_2 = ln(2)/pole = 6.8628\,s$. Based on the provided table from the course notes [1], it's evident that the spiral mode classification follows certain criteria. Initially, to be categorized as level 1, the value of T_2 must exceed 12 seconds, which is not the case. Consequently, progressing to level 2, the threshold shifts to $T_2 > 8\,s$, still unmet. Similarly, for level 3, the requirement is $T_2 > 5\,s$. Given that $T_2 = 6.8628$ seconds, surpassing this threshold for level 3, it is classified as level 3 in the spiral mode.

Roll Subsidence

In the case of roll subsidence, where the maximum time constant is $t_{max} = 0.0564\,s$, to classify it as level 1, t_{max} would need to be less than$1s$, a condition that is indeed met. Hence, the roll subsidence mode is characterized as level 1.

Dutch Roll

Regarding the dutch roll mode, characterized by parameters $\xi = 0.0607$ and $w_n = 5.35\,rad/s$, along with $\xi w_n = 0.325\,rad/s$, the conditions for level 1 are assessed: $\xi > 0.19$, $w_n > 1\,rad/s$, and $\xi w_n > 0.35\,rad/s$. While w_n meets the criterion, the others do not, prompting us to move to level 2. Here, the criteria are: $\xi > 0.002$, $w_n > 0.5\,rad/s$, and $\xi w_n > 0.05\,rad/s$, all of which are satisfied since $\xi = 0.0607 > 0.002$, $w_n = 5.35\,rad/s > 0.5\,rad/s$, and $\xi w_n = 0.325\,rad/s > 0.05\,rad/s$. Therefore, it is classified as level 2.

Ultimately, the aircraft's stability is determined by the highest level among the three modes. Therefore, this aircraft exhibits a lateral stability of level 3.

3. Stability Augmentation System

In order to enhance aircraft maneuverability and ensure optimal flight characteristics, specifically achieving a level 1 stability, the implementation of a Stability Augmentation System (SAS) is imperative. This system aims to address the following objectives:

- For the dutch roll mode, currently classified as with level 2 stability, a yaw feedback mechanism will be introduced. This mechanism aims to increase the damping ratio above 0.6 and adjust these parameters to meet the criteria for level 1 stability.

- The spiral divergence mode is unstable due to a pole in the Right Half Plane. Introducing a yaw feedback for dutch roll is expected to shift this pole to the LHP, optimally. If this doesn't stabilize the system and thus classify it as a level 1 stability mode, further adjustments will be made.

- Lastly, it is crucial to ensure that, following the adjustments, the subsidence roll mode maintains stability at level 1. If this is not the case, necessary modifications will be carried out to guarantee stability at this level.

Yaw Damper

Taking these points into account, the process starts with implementing yaw feedback for dutch roll. To achieve this, the state r will be fed back into the system using $C = [0\,0\,1\,0]$, where only the second column of B will be considered to isolate δ_R as an input. With this setup, the following transfer function was obtained:

$$\frac{r}{\delta_R} = \frac{22.18s^3 + 398s^2 + 66.75s + 644.4}{s^4 + 18.28s^3 + 38.23s^2 + 502.7s - 51.32}$$

Since not all the coefficients of the denominator have the same sign, this transfer function describes an unstable system.

By feeding the yaw rate back to the system the following *rootlocus* was obtained:

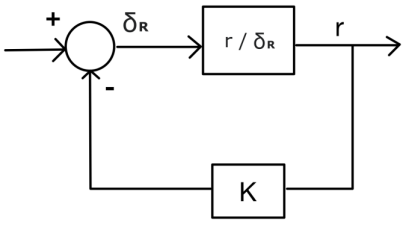

Figure 1: SAS of dutch roll yaw damper

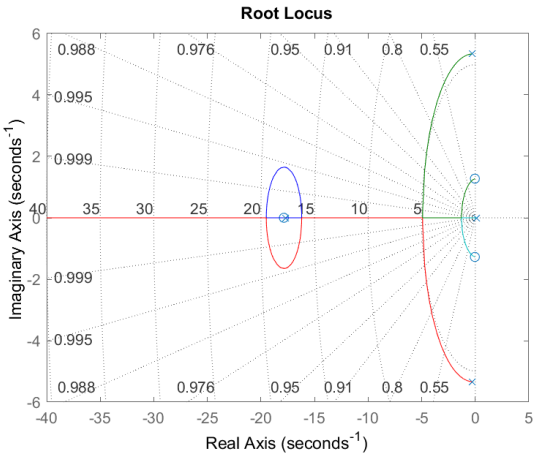

Figure 2: Rootlocus of yaw rate / rudder transfer function

As mentioned earlier, the goal is for this yaw feedback to not only impact the dutch roll mode but also stabilize the spiral divergence mode by altering its pole to be located in the LHP, in the best case scenario. Thus, it was found that, for the spiral mode, in order for its pole to be a negative real pole, the associated gain would need to fall within the range of $0.0797\,s < K < 0.574\,s$.

Regarding the roll subsidence mode, which was already at level 1 stability, it was desired that there would be no alteration in its level. Initially, the limits regarding the gain for which the pole would remain a real pole were analyzed. These limits correspond to $0\,s < K < 0.722\,s$ or $K > 0.995\,s$, although only the first interval will be considered, as it is within this interval that the gain condition for the spiral mode is satisfied. Within the analysed range, the maximum time constant increases with the gain, reaching its maximum value $t_{max} = 0.0617\,s$ for $K_r = 0.722\,s$. Since this value satisfies the condition for level 1 roll subsidence mode ($t_{\max} < 1\,s$), it is concluded that the roll subsidence mode will maintain its level 1 stability for any gain within this interval.

Additionally, for the required minimum damping coefficient of $\xi > 0.6$ for the dutch roll mode, the corresponding gain condition is $K > K_{\xi=0.6} = 0.267\,s$.

Therefore, by integrating these criteria, the damping coefficient $\xi = 0.8$ corresponding to $K = 0.3577\,s$ was selected for the dutch roll mode. The new transfer function of the yaw rate response due to rudder input with the yaw damper as seen on figure1 is given by:

$$\frac{r}{\delta_R} = \frac{22.18s^3 + 398s^2 + 66.75s + 644.4}{s^4 + 26.21s^3 + 180.6s^2 + 526.6s + 179.2}$$

This transfer function has all of its denominator coefficients with the same sign, which, although not

sufficient, it is a necessary condition for the system to be stable. The new poles can be obtained by using the *damp* function in Matlab on the closed-loop dynamic system $A - B_{\delta_R} KC$:

Flight modes	poles	ξ	w_n $[rad/s]$	time const.[s]
Spiral divergence	-0.389	1.00	0.389	2.57
Dutch roll	$-4.09 \pm 3.05i$	0.802	5.11	0.244
Roll subsidence	-17.6	1.00	17.6	0.0567

Table 2: SAS lateral mode results

Regarding the dutch roll mode, it is observed that $\xi = 0.802 > 0.19$, $w_n = 5.11\, rad/s > 1\, rad/s$, and $\xi w_n = 4.098\, rad/s > 0.35\, rad/s$, thus satisfying the level 1 stability conditions for this mode. Consequently, the dutch roll mode is of level 1 stability.

Referring to the table, it is evident that through yaw feedback for dutch roll, the spiral divergence mode is also altered to achieve stability, now with a negative real pole $p = -0.389$, thereby confirming it as level 1 mode.

Lastly, for the roll subsidence mode, it is observed that the maximum time constant satisfies the stability condition for level 1 - $t_{max} = 0.0567s < 1s$, indicating that this mode is also at level 1 stability.

In conclusion, the aircraft's stability is determined by the highest level among the three modes. Therefore, this aircraft exhibits a lateral stability of level 1, and thus successfully confirming that the goals were met.

4. Attitude/trajectory control

The objective of this section is to develop a control system that enables the control of the attitude and trajectory of the UAV. An emphasis will be given to the sideslip and roll angles.

To accomplish this goal, one of the optimal control methods was chosen, the Linear Quadratic Regulator (LQR), where the controller is derived through an optimization process aimed at minimizing the cost function J:

$$J = \frac{1}{2} \int_0^\infty (x^T Q x + u^T R u)\, dt$$

In this regard, it is necessary to define the weighting matrices for states and inputs, Q and R, respectively. Initially, the Bryson method was employed to establish initial values for these matrices, which were subsequently fine-tuned to improve the closed-loop system's performance.

One simple solution for control systems is the servomechanism [1], which was created as seen below:

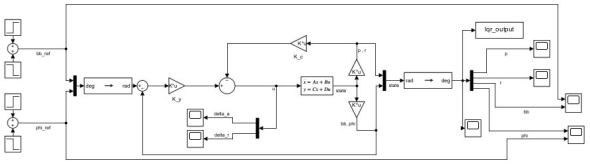

Figure 3: LQR servomechanism

During this process the following matrix C was used in order to control the desired variables β and ϕ, and D is simply zero since the input does not directly influence the output:

$$C = \begin{bmatrix} 1 & 0 & 0 & 0 \\ 0 & 0 & 0 & 1 \end{bmatrix}$$

$$D_{(2\times 2)} = 0_{(2\times 2)}$$

The Q and R matrices can be defined by using the Bryson method, where:

$$Q = diag(Q_i), \text{ with } Q_i = \frac{1}{x_{i,max}^2}$$

$$R = diag(R_i), \text{ with } R_i = \frac{1}{u_{i,max}^2}$$

The vectors $x_{i,max}$ and $u_{i,max}$ were defined as:

$$x_{max} = [0.1 \;\; 0.5 \;\; 0.3 \;\; 0.25]^T$$

$$u_{max} = [0.1\delta_{A_{max}} \;\; 0.1\delta_{R_{max}}]^T = [0.0524 \;\; 0.0785]^T$$

Therefore, the resulting Q and R matrices are:

$$Q = \begin{bmatrix} 100 & 0 & 0 & 0 \\ 0 & 4 & 0 & 0 \\ 0 & 0 & 11.1 & 0 \\ 0 & 0 & 0 & 16 \end{bmatrix}$$

$$R = \begin{bmatrix} 365 & 0 \\ 0 & 162 \end{bmatrix}$$

The following gain was obtained using the *lqr* function:

$$K_{LQR} = \begin{bmatrix} 0.0843 & -0.0321 & 0.0054 & -0.1929 \\ -0.3511 & -0.0100 & 0.2964 & 0.1100 \end{bmatrix}$$

Flight modes	poles	ξ	w_n $[rad/s]$	time const.[s]
Spiral divergence	-19.2	1.00	19.2	0.0520
Dutch roll	$-3.48 \pm 4.68i$	0.5972	5.83	0.287
Roll subsidence	-1.01	1.00	1.01	0.990

Table 3: Lateral mode poles for LQR servomechanism

The poles which represent the feedback $A - B\,K_{lqr}$ define a stable aircraft with its lateral modes still identifiable.

Having the LQR gain, one may define:

$$\mathrm{K}_y = \begin{bmatrix} 0.0843 & -0.1929 \\ -0.3511 & 0.1100 \end{bmatrix} \; K_c = \begin{bmatrix} -0.0321 & 0.0054 \\ -0.0100 & 0.2964 \end{bmatrix}$$

by extracting the columns of K_{LQR} that represent each variable to its according gain vector (K_y for β and ϕ and K_c for the complementary variables).

Putting everything together, the LQR servomechanism outputs these results for a interspersed reference of $[\beta_{ref}\,\phi_{ref}]^T = [5 \quad 0]^T\,^\circ$ and $[0 \;\; 25]^T\,^\circ$:

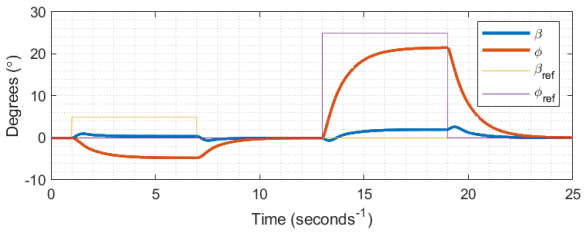

Figure 4: LQR servomechanism with variables response: $\beta[^\circ]$, $\phi[^\circ]$.

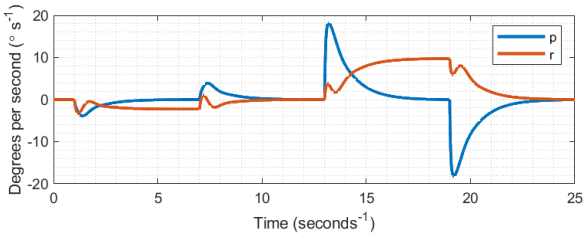

Figure 5: LQR servomechanism with variables response: $p[^\circ/s]$, $r[^\circ/s]$.

One can easily conclude that the system converges to a specific state, but that it does not converge to the reference values.

A good way to reduce this static error is to add integrative variables. To do this, a simple gain with an integrator can be added in parallel with the gain associated with output variables β and ϕ. The state is now defined by $x = [\beta \quad p \quad r \quad \phi \quad \int\beta \quad \int\phi]^T$ and the matrices A and B are changed to the following structure:

$$A = \begin{bmatrix} Y_\beta & Y_p + \tan\alpha_0 & Y_r - 1 & \frac{g\cos\theta_0}{U_0} & 0 & 0 \\ L'_\beta & L'_p & L'_r & 0 & 0 & 0 \\ N'_\beta & N'_p & N'_r & 0 & 0 & 0 \\ 0 & 1 & \tan\theta_0 & 0 & 0 & 0 \\ 1 & 0 & 0 & 0 & 0 & 0 \\ 0 & 0 & 0 & 1 & 0 & 0 \end{bmatrix}$$

$$B = \begin{bmatrix} Y_{\delta_A} & Y_{\delta_R} \\ L'_{\delta_A} & L'_{\delta_R} \\ N'_{\delta_A} & N'_{\delta_R} \\ 0 & 0 \\ 0 & 0 \\ 0 & 0 \end{bmatrix}$$

The two new state variables will imply that the Q matrix is now of size (6×6):

$$Q = \begin{bmatrix} 100 & 0 & 0 & 0 & 0 & 0 \\ 0 & 4 & 0 & 0 & 0 & 0 \\ 0 & 0 & 11.1 & 0 & 0 & 0 \\ 0 & 0 & 0 & 16 & 0 & 0 \\ 0 & 0 & 0 & 0 & 1 & 0 \\ 0 & 0 & 0 & 0 & 0 & 1 \end{bmatrix}$$

It is important to note that the values which correspond to the integrative values should have an order of magnitude inferior to those which they represent, that is β and $\int\beta$, for example.

R stays the same since there is no change in the input variables of the system.

A new gain may be obtained using the same method as before. The gain is now of size (2×6):

$$\mathrm{K}_{LQR} = \begin{bmatrix} 0.0892 & -0.0340 & 0.0031 & -0.2351 & -0.0342 & -0.0397 \\ -0.3756 & -0.0085 & 0.3014 & 0.1501 & -0.0595 & 0.0512 \end{bmatrix}$$

Thus, one may evaluate the corresponding poles of the resulting servomechanism:

Flight modes	poles	ξ	w_n $[rad/s]$	time const.[s]
–	-0.0437	1.00	0.0437	22.9
–	-0.238	1.00	0.238	4.19
Spiral divergence	-0.982	1.00	0.983	1.02
Dutch roll	$-3.48 \pm 4.68i$	0.597	5.83	0.287
Roll subsidence	-19.2	1.00	19.2	0.0520

Table 4: Lateral mode poles for LQR servomechanism with integrative variables

Two new poles surge due to the addition of the integrative variables. The lateral modes are still identifiable, having none of them being degenerated.

K_y and K_c are obtained the same way they were before:

$$\mathrm{K}_y = \begin{bmatrix} 0.0892 & -0.2351 \\ -0.3756 & 0.1501 \end{bmatrix} \; K_c = \begin{bmatrix} -0.0340 & 0.0031 \\ -0.0085 & 0.3014 \end{bmatrix}$$

The gains which correspond to the integrative variables are the last two columns, making it a (2×2) matrix as before:

$$K_i = \begin{bmatrix} -0.0342 & -0.0397 \\ -0.0595 & 0.0512 \end{bmatrix}$$

The following servomechanism can be applied with these matrices:

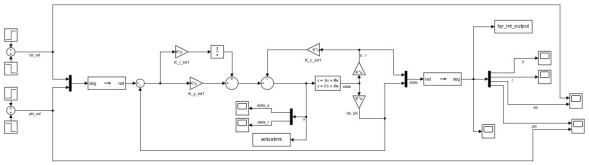

Figure 6: LQR servomechanism with integrative variables

For interspersed reference of $[\beta_{ref}\ \phi_{ref}]^T = [5\ \ 0]^T\ ^\circ$ and $[0\ \ 25]^T\ ^\circ$, the result was:

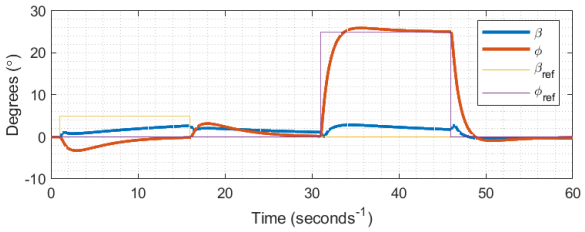

Figure 7: LQR servomechanism with integrative variables response: $\beta\ [^\circ]$, $\phi\ [^\circ]$.

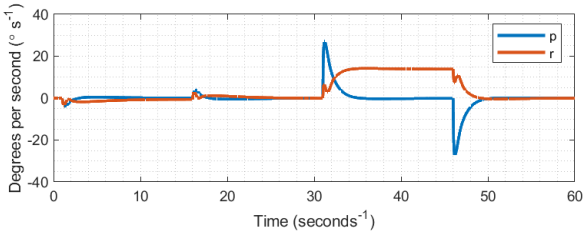

Figure 8: LQR servomechanism with integrative variables response: $p\,[^\circ/s]$, $r\,[^\circ/s]$.

The state variable ϕ converges to the reference values and β only reaches a value which is close to the reference value in the presented time frame. For a longer simulation time, the system does converge to the desired value. Adjusting the matrices Q and R could be a simple solution for this. However, one should be aware of not compromising the other variables responses.

The roll rate p converges to 0 and the yaw rate r converges to a value different from 0. This implies that the aircraft begins a turn and tends to turn at a constant angular speed. This is useful for trajectory control and similar concepts will be used in the next sections of the paper for the patrol mission.

The system has a very rapid response. Since this is an unmanned aerial vehicle, there is no problem regarding G forces, as long as the aircraft is designed to sustain these accelerations.

Another interesting thing to analyse is the actuation response of the signals δ_A and δ_R:

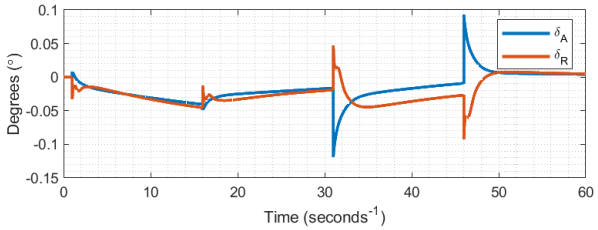

Figure 9: Actuation signals: $\delta_A[^\circ]$ $\delta_R[^\circ]$

The actuators keep changing their signal over time, due to the reference value of β not being met in the time frame shown. Therefore, the controller is still trying to find a solution which meets both reference points given to the system. Again, by changing the matrices Q and R this could be changed, but there should be special attention given to the overall system response.

5. Sensors and Actuators

The sensors and actuators, used to transmit information between the aircraft and the controller, are fundamental elements whose quality, precision and reliability, allow (or limit) and dimensionthe quality of the achieved control. In the previous sections of this report, sensors and actuators were considered ideal, meaning there was no presence of noise, and they responded instantaneously. However, in reality, this is not the case, so their dynamics must be considered. For this reason, it was necessary to add non-ideal sensors and actuators from this point onwards.

Actuators

Excluding the propulsive force, the actuators in flight control are aimed at positioning the control surfaces. In this report, these surfaces are the ailerons and the rudder, whose respective angles correspond to the inputs of the system, δA and δR, respectively.

When modeling these actuators, certain limitations and parameters had to be taken into account. With the aid of a *Saturation* block in *SIMULINK*, the deflection angles of the ailerons and the rudder were limited to $(\delta A)_{max} = 30^o$ and $(\delta R)_{max} = 45^o$, respectively. A *Rate Limiter* was used to define a maximum speed of $30^\circ/s$, as well as a *Zero-Order Holder* to introduce the sampling frequency of 100Hz. Since the actuator dynamics are often approximated as a simple first-order low-pass filter,

a transfer function $\frac{1}{Ts+1}$ was added, with the time constant being $T = 40ms$.
Thus, the following block diagram was obtained:

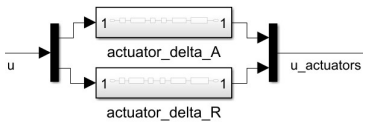

Figure 10: Block diagram for actuators

The model for both δ_A and δ_R actuators is the same since the parameters are identical. Thus, the following model was obtained for these actuators:

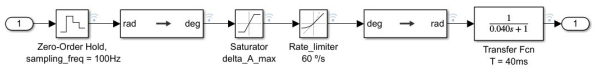

Figure 11: Actuator for δ_A

Given that the transfer function describing the actuators' dynamics has a unity gain, it implies that the output signal accurately mirrors the input signal with a small delay in time.

Sensors

From the wide array of available sensors, only the following sensors needed to be modeled due to the requirements of the patrol mission:

- Sensor for roll and pitch rates, p and r;
- Sensor for roll angle, ϕ;
- Sensors for aircraft position and velocity via GPS;

These sensors operate at a frequency of $f = 100$Hz, except for the GPS-based velocity sensor, which operates at a sampling frequency of 5Hz, introduced using a *Zero-Order Holder*. When necessary, tools such as *Quantizer* were used for resolutions (e.g.$0.5m$), and *Saturator* for limitations (e.g. $300°/s$).

For the values of root mean square (rms) and least significant bit for noise (LSB_{rms}), the *Band-Limited White Noise* tool was utilized. The parameters for *noise power* were obtained using the following expressions:

$$NP = \frac{rms^2}{freq}$$

$$NP = \frac{(LSB_{rms}\frac{V_{dc_2} - V_{dc_1}}{2^N})^2}{freq}$$

Sensors for roll rate, yaw rate and roll angle

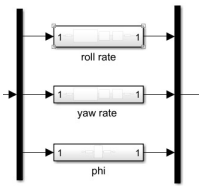

Figure 12: Sensors for p , r and ϕ.

The sensors for the angular rates p and r are identical because they share the same parameters. Since these are analog sensors, it was necessary to incorporate a digital converter. Subsequently, an inverter was employed to convert the signal from voltage to the desired units. The model is as follows:

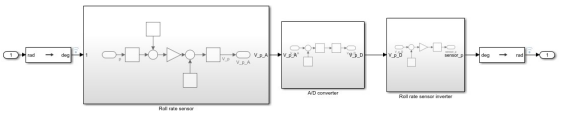

Figure 13: Sensor blocks for roll rate.

Starting with the sensor itself, one was created with saturation at $\pm 300°/s$ and an rms of $4.4°/s$ using the aforementioned tools. This sensor also had a voltage limitation of $[0.7 - 4.3]V_{dc}$. Therefore, to ensure that the initial input values were within the saturation range, a gain was introduced to convert from degrees to voltage. This gain value was obtained by the ratio between the voltage and degree limitations, $\frac{4.3-0.7}{300-(-300)}V/(°/s)$. Thus, the following block diagram was obtained:

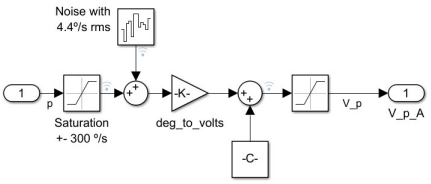

Figure 14: Roll rate sensor.

With the assistance of the analog-to-digital converter AD depicted in the following image, the signal was converted into voltage. Since only the sensors for the angular rates are analog, the converter was solely utilized for these sensors.

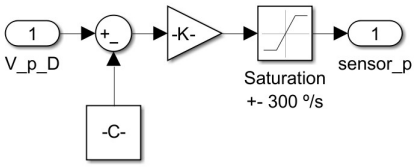

Figure 15: AD converter.

As the signal output from the converter is in voltage, an inverter was necessary to convert the voltage signal back to real values. Consequently, an inverter was implemented for the roll and yaw rates to convert the obtained values back to the desired units ($^\circ/s$).

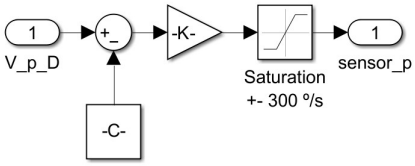

Figure 16: Inverted sensor for roll rate.

For the ϕ sensor, with digital output, it was only necessary to consider the parameters for resolution, 0.1°, and rms, 0.3°. The following block diagram was obtained:

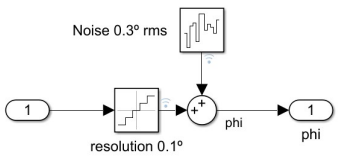

Figure 17: Sensor for roll angle.

Global Positioning System (GPS)

For the GPS, two sensors were required: one for velocity and another for position, as depicted in the following image.

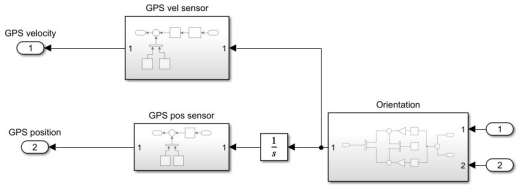

Figure 18: GPS

Regarding the orientation block, it was used to obtain the velocity of the aircraft. The heading angle $\beta + \psi$ was considered, and consequently, the velocities in the North and East directions were given by $V_N = U_0 \cos(\beta + \psi)$ and $V_E = U_0 \sin(\beta + \psi)$, respectively. It is noteworthy that the wind velocity was taken into account by adding it to the respective components of the aircraft's velocity. In this case, the wind velocity is constant, $3\,m/s$, at $-15°$.

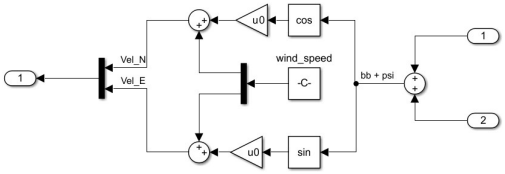

Figure 19: Orientation for GPS

With these values, we have the velocity, and for the position, it is sufficient to integrate them. Regarding the sensors, both the velocity and position sensors have the same format, including resolution and noise, with the exception of the position sensor, which also requires introducing a sampling frequency of 5Hz. Thus, the following position sensor was obtained:

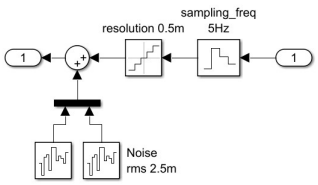

Figure 20: GPS position sensor.

Estimator

As there is no direct sensor for the sideslip angle β, a state estimator based on Kalman filtering theory was used, which receives the remaining 3 state

variables (p, r and ϕ) from the sensors and estimates a value for β. This was incorporated into the system as follows:

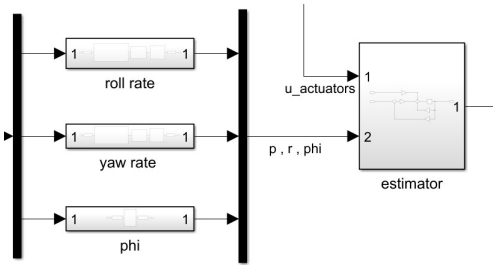

Figure 21: Location of the estimator.

During this process, the Kalman gain L was calculated. The following matrix C_e was utilized to control the desired variables for the input of the estimator (p, r and ϕ).

$$C_e = \begin{bmatrix} 0 & 1 & 0 & 0 \\ 0 & 0 & 1 & 0 \\ 0 & 0 & 0 & 1 \end{bmatrix}$$

The remaining matrices $G_0 = I_{4\times4}$, $Q_0 = 0.01I_{(4\times4)}$ and $R_0 = 0.01I_{(3\times3)}$ were used to calculate the Kalman gain. With this, the following gain was obtained using the *lqe* function, $L = lqe(A, G_0, C_e, Q_0, R_0)$:

$$L = \begin{bmatrix} -0.5073 & 0.2990 & 0.0151 \\ 1.5395 & -0.4221 & 0.0219 \\ -0.4221 & 3.5848 & -0.0266 \\ 0.0219 & -0.0266 & 1.0209 \end{bmatrix}$$

With this, the following estimator was ultimately defined:

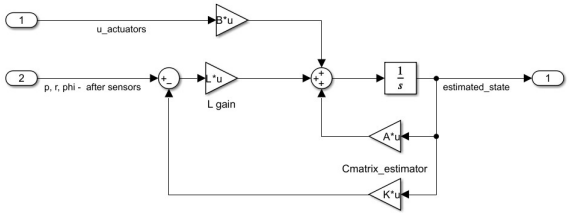

Figure 22: Estimator.

This estimator not only acted as a substitute for a sensor for β, but also mitigated disturbances in the other state variables p, r, and ϕ, obtained after passing through the sensors. Consequently, the noise was significantly reduced, as demonstrated by the following image for the roll rate:

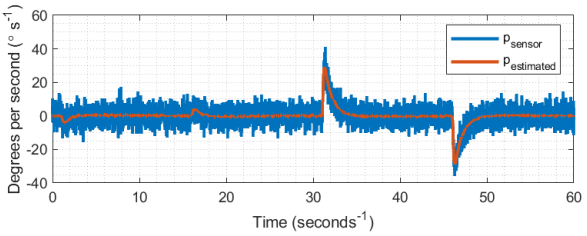

Figure 23: Variation of roll rate with estimator.

Simulation results

After the integration of actuators and sensors into the system, the following response of inputs and states was obtained for interspersed reference of $[\beta_{ref}\ \phi_{ref}]^T = [5\ \ 0]^T\,^\circ$ and $[0\ \ 25]^T\,^\circ$:

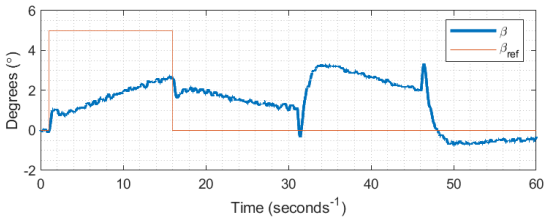

Figure 24: β interspersed reference of $[\beta_{ref}\ \phi_{ref}]^T = [5\ \ 0]^T\,^\circ$ and $[0\ \ 25]^T\,^\circ$.

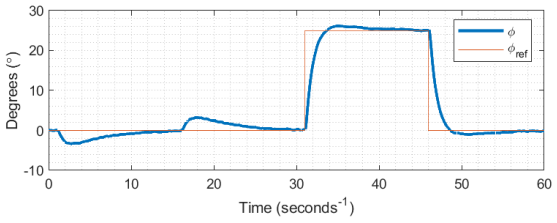

Figure 25: ϕ interspersed reference of $[\beta_{ref}\ \phi_{ref}]^T = [5\ \ 0]^T\,^\circ$ and $[0\ \ 25]^T\,^\circ$.

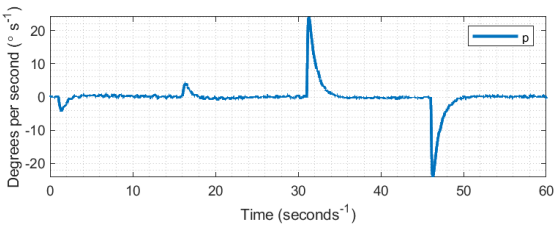

Figure 26: Roll rate interspersed reference of $[\beta_{ref}\ \phi_{ref}]^T = [5\ \ 0]^T\,^\circ$ and $[0\ \ 25]^T\,^\circ$.

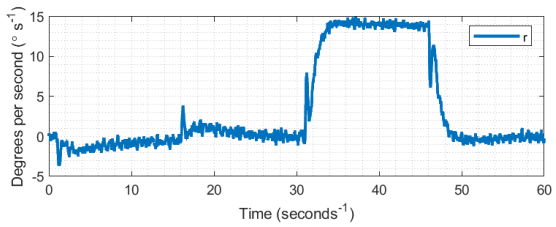

Figure 27: Yaw rate interspersed reference of $[\beta_{ref}\ \phi_{ref}]^T = [5\ \ 0]^T\,^\circ$ and $[0\ \ 25]^T\,^\circ$.

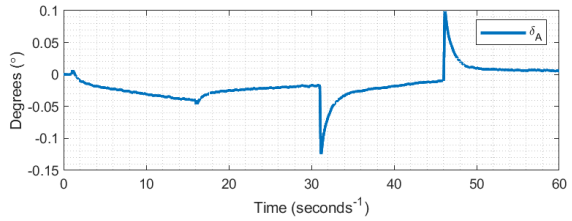

Figure 28: δ_A interspersed reference of $[\beta_{ref}\ \phi_{ref}]^T = [5\ \ 0]^T\,^\circ$ and $[0\ \ 25]^T\,^\circ$.

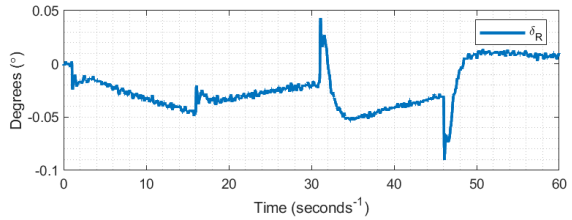

Figure 29: δ_R interspersed reference of $[\beta_{ref}\ \phi_{ref}]^T = [5\ \ 0]^T\,^\circ$ and $[0\ \ 25]^T\,^\circ$.

6. Patrol maneuver

As a final objective for this project, a patrol mission was aimed to be performed. The figure below illustrates the desired path:

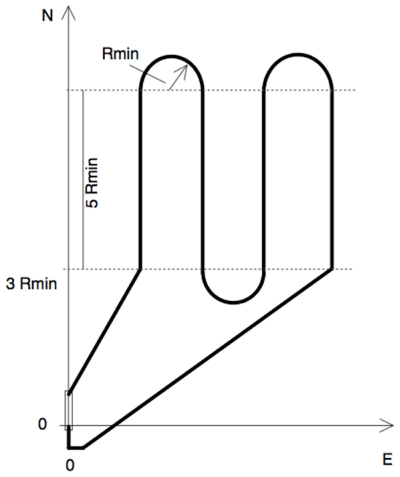

Figure 30: Patrol trajectory

For this, the L1 guidance method for UAVs was chosen as the algorithm used for path control. This method is described by the use of a correction angle for the flight path angle in order to align the aircraft with the desired trajectory:

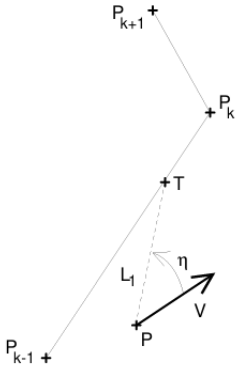

Figure 31: L1 tracking method

To correct this angle, a lateral acceleration can be used:

$$a_y^d = \frac{2V^2}{L_1}\sin\eta$$

The η angle represents the error angle between the aircraft's velocity and direction of the L1 point from the desired path. L_1 was defined to be 3.5 times the distance the aircraft travels at constant speed U_0.

Assuming the turning maneuvers as coordinated turns, this acceleration can be converted into a reference value for the roll angle by dividing the given acceleration by the gravity:

$$\phi_{cmd} = \frac{a_y}{g}$$

To do this, the North direction was chosen as the reference direction of the plane. The *atan2* function came in handy for the calculation of the angle based on the 4 quadrants. This function was used both in the calculation of the current heading and L1 reference heading. The η angle can then be obtained by subtracting the current heading from the L1 reference heading. The positive signal represents a right turn and a negative signal a left turn. However, this only works when the aircraft is facing North because discontinuities arise when the absolute value of the angle is greater than 90°. To avoid these imprecisions, the coordinate system for the vectors can be inverted and by making the error angle now the difference between the current heading and the L1 reference heading.

One thing to be noted is that there will be generally two points which have a distance of L_1 meters from the current aircraft's position. To choose the

correct, one may simply evaluate if the L_1 point is located in from of the UAV or behind it. In other words, check if the absolute value of η is smaller than 90°.

To obtain the points which best describe the desired path, the following waypoints for the flight were chosen:

East [meters]	North [meters]	Angle [degrees]
0	0	90
0	$1R_{min}$	90
$2R_{min}$	$3R_{min}$	90
$2R_{min}$	$8R_{min}$	90
$3R_{min}$	$9R_{min}$	0
$4R_{min}$	$8R_{min}$	-90
$4R_{min}$	$3R_{min}$	-90
$5R_{min}$	$2R_{min}$	0
$6R_{min}$	$3R_{min}$	90
$6R_{min}$	$8R_{min}$	90
$7R_{min}$	$9R_{min}$	0
$8R_{min}$	$8R_{min}$	-90
$8R_{min}$	$3R_{min}$	-90
$1.5R_{min}$	$-1R_{min}$	-180
$0.95R_{min}$	$-1R_{min}$	180
0	0	90

Table 5: Way points

The velocity of the UAV, U_0, remained constant throughout the trajectory. To define R_{min}, the circular portion of the patrol trajectory, made at constant speed, was considered. Thus, the centripetal acceleration in equilibrium is given by:

$$a_c = \omega U_0 = \frac{V^2}{R}$$

With ω being defined by $\omega = \frac{g}{U_0} tan(\phi)$, combining these equations yields the following expression for calculating the minimum radius for the UAV trajectory:

$$\frac{V^2}{R_{min}} = [\frac{g}{U_0} tan(\phi)]\, U_0 \Leftrightarrow$$

$$\Leftrightarrow R_{min} = \frac{U_0^2}{9.81 \tan(\phi_{max})}$$

A slightly smaller angle than ϕ_{max} was chosen to guarantee that the UAV is able to perform the coordinated turns accordingly. Therefore the expression for R_min used was:

$$R_{min} = \frac{U_0^2}{9.81 \tan(\phi_{max} - 7)} = 105.8\,\text{m}$$

The heading angle for the aircraft was assumed to be $\psi + \beta$, however, since the reference value for the sideslip angle β is always set to 0 in the controller, the angle can be approximated to the yaw angle, *heading angle* $\approx \psi$. The orientations on the third column of the table are the desired ones at the given point.

The following image represents the *Simulink* block for the L1 method:

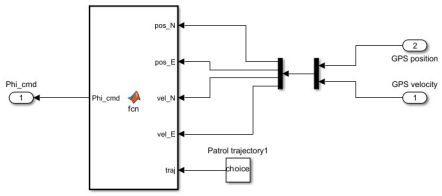

Figure 32: L1 tracking method

Within this block, there is a function that receives the velocity and position provided by the GPS, as well as the intended trajectory for the UAV (*choice*). Using the L1 tracking method, this function determines the next point to follow in the trajectory, calculates the associated angle η, and determines the angle ϕ_{cmd} to be fed back into the system as the reference for the roll angle.

In order for the L1 method to be performed, an extrapolation between each waypoint will need to be performed. For this, two methods were tested. One method assumes that the path between each waypoint is described by a simple straight line. There are only three occasions where a circumference is assumed and can be easily spotted in figure 30. Besides this being the simplest approach to design the UAV's flight trajectory, it also gives an extra challenge to the aircraft when reaching a waypoint whose path lines have a very different orientation. This results in very sharp turns from the perspective of the UAV as can be seen in the simulation:

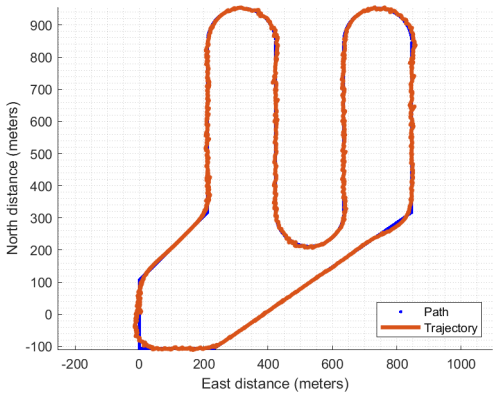

Figure 33: UAV trajectory analysis for trajectory 1.

A good way to tackle this is by assuming an extrapolation between waypoints which in turn can be represented by differentiable functions. To do this, the *dubinsSpace* robotics package was used to obtain the path. Below is the resulting simulation with this new path:

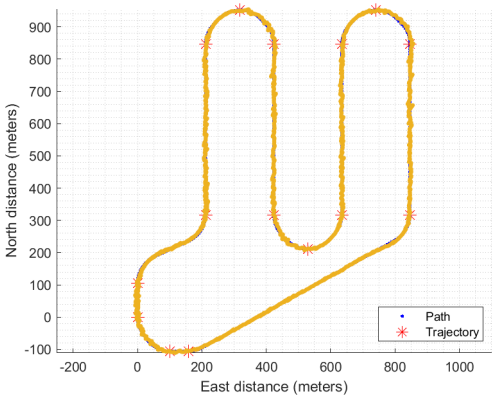

Figure 34: UAV trajectory analysis for trajectory 2.

It can be seen that this flight path can be better performed by the UAV as no sharp turns are to be found. There is a precision of around 10 meters meters in the trajectory following.

Here the reference values for the roll angle ϕ can be seen. Only when initiating the coordinated turns which positioned the aircraft in a 180° turn does ϕ_{cmd} saturate. For safety measures, the saturation limit was chosen to be ±29° so that it does not reach the 30° limit present in the projects' reference paper [2].

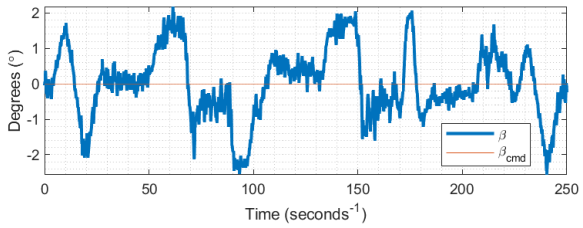

Figure 35: Sideslip angle (β) analysis.

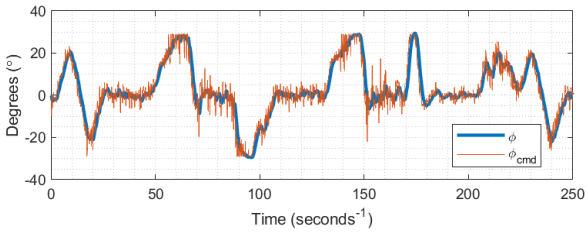

Figure 36: Roll angle (ϕ) analysis .

Additionally, one can see that although the reference value for the sideslip angle β was always set to zero in order to perform coordinated turns along the flight, the angle was oscillating between ±2 degrees throughout the entirety of the flight.

7. Conclusion/Critical analysis

All project objectives were met successfully, demonstrating the effectiveness of the endeavor.

These final simulations show that the UAV can perform the patrol mission with very good precision.

The estimator used in section 5 was not fine-tuned since the weight matrices for states and inputs, Q and R respectively, have random equal numbers. For a slightly better performance of the state estimation of the aircraft's flight characteristics, the Kalman filter can be optimized for this matter.

One thing to be noted in the coordinate system used in the patrol maneuver is that there may be more imprecision in the results when the aircraft is orientated to either East or West. This is due to the coordinate system inversion used when the velocity in the North component inverts its signal. If the UAV is oriented along the East axis, then it is very likely that it will be switching coordinate systems frequently. Despite this, no problems arose with this method in this simulation.

Further development

As part of a continuation of this work, and still considering the lateral movement of the aircraft, would be to have in consideration the physics of the take-off and landing maneuvers.

Although the UAV is able to follow the path trajectory considerably well in every part of the flight, the aircraft should not take use of the ailerons as a source for turning the vehicle while it is still on the ground.

Regarding the longitudinal movement of the aircraft, one may design a controller to control the altitude, velocity, and other characteristics of the flight of the UAV. For take-off and landing, these would be very useful. The integration of the lateral and longitudinal movements of the aircraft would allow for full control of the aircraft in the 3D environment.

References

[1] J. R. Azinheira. *Controlo de Voo*. 2024.

[2] J. R. Azinheira. *Enunciado dos projectos 2023-2024*. 2024.